

Probing violation of the Copernican principle via the integrated Sachs-Wolfe effect

Kenji Tomita

Yukawa Institute for Theoretical Physics, Kyoto University, Kyoto 606-8502, Japan

Kaiki Taro Inoue

Department of Science and Engineering, Kinki University, Higashi-Osaka, 577-8502, Japan

(Dated: November 5, 2018)

Recent observational data of supernovae indicate that we may live in an underdense region, which challenges the Copernican principle. We show that the integrated Sachs-Wolfe (ISW) effect is an excellent discriminator between anti-Copernican inhomogeneous models and the standard Copernican models. As a reference model, we consider an anti-Copernican inhomogeneous model that consists of two inner negatively curved underdense regions and an outer flat Einstein-de Sitter region. We assume that these regions are connected by two thin-walls at redshifts $z = 0.067$ and $z = 0.45$. In the inner two regions, the first-order ISW effect is dominant and comparable to that in the concordant flat- Λ models. In the outer Einstein-de Sitter region, the first-order ISW effect vanishes but the second-order ISW effect plays a dominant role, while the first-order ISW effect is dominant in the flat- Λ models at moderate redshifts. This difference can discriminate the anti-Copernican models from the concordant flat- Λ model. At high redshifts, the second-order ISW effect is dominant both in our inhomogeneous model and the concordant model. In the outer region, moreover, the ISW effect due to large-scale density perturbations with a present matter density contrast $\epsilon_{m0} \ll 0.37$ is negligible, while the effect due to small-scale density perturbations (such as clusters of galaxies, superclusters and voids) with $\epsilon_{m0} \gg 0.37$ would generate anisotropies which are larger than those generated by the ISW effect in the concordant model.

PACS numbers: 98.80.-k, 98.70.Vc, 04.25.Nx

I. INTRODUCTION

Assuming a uniform distribution of matter on large scales, the observed data of high-redshift type Ia supernovae (SNIa)[1, 2, 3, 4] point to Λ -dominated flat Friedmann-Robertson-Walker (FRW) models. The darkness of the SNIa is reduced to accelerating expansion of the universe due to a positive Λ term.

These Λ -dominated FRW models are consistent also with the observed data of temperature anisotropy in the Cosmic Microwave Background (CMB) radiation[5, 6], except for the low-multipole components[7, 8]. Moreover the observed correlation between the CMB and large-scale structure supports these Λ -dominated models, which can generate anisotropies due to the first-order(linear) ISW effect[9, 10, 11].

On the other hand, alternative inhomogeneous models that can explain the SNIa data without introducing a cosmological constant Λ have been independently proposed by C el erier[12], Goodwin et al.[13] and Tomita[14, 15, 16, 17] and subsequently studied by several authors[18, 19, 20, 21]. It turned out that some inhomogeneous cosmological models with an inner large-scale underdense region (which we called *a local void* in our previous works) with a small Hubble constant ($h \approx 0.5$) in the outer flat region can also explain the CMB data[18, 20, 22, 23] as well as the SNIa data. In these models, the cosmological Copernican principle is violated since we need to live near the center of an underdense region.

However, recent observational studies such as the baryon acoustic oscillations (BAO)[24, 25, 26, 27, 28, 29, 30], the kinematic Sunyaev-Zeldovich effect either from clusters [31] or reionized regions[32] put stringent constraints on these anti-Copernican models. As a result, models with a local void on 300 Mpc scales seem to be ruled out. At the moment, we need to consider inhomogeneous models with a local void on Gpc scales so that the constraints from BAO at epochs of $z \leq 0.45$ may be avoided. Recently several Gpc void models have been studied by Clifton et al.[33] and Garc ia-Bellido and Haugb olle[34].

In this paper we study the ISW effect¹ in flat FRW models with an inner underdense region on Gpc scales based on previous results[35, 36, 37, 38, 39, 40]. Then we compare it with the ISW effect in the concordant flat FRW model with a cosmological constant Λ . As we shall show, the ISW effect will be an excellent discriminator

¹ In this paper, “the ISW effect” means redshift/blueshift of the CMB photons due to time-evolving first-order or second-order metric perturbations.

between our anti-Copernican models and the standard concordant Copernican model. In §2, we present our inhomogeneous cosmological model with inner underdense regions and in §3 we derive analytic formulae for calculating the ISW effect in the inner and outer regions and we discuss the property of temperature anisotropy due to the ISW effect in our models and the concordant model. §4 is dedicated to concluding remarks. In what follows, we use the units of $8\pi G = c = 1$. For spatial coordinates, we use Latin subscripts running from 1 to 3.

II. A COSMOLOGICAL MODEL WITH INNER UNDERDENSE REGIONS

Our inhomogeneous anti-Copernican models without a cosmological constant Λ consist of two inner underdense regions (I and II) and an outer flat region (III). The former regions are described by negatively curved FRW models ($\Omega_{I0} = 0.3$ and $\Omega_{II0} = 0.6$) and the outer region is by the Einstein-de Sitter model (EdS) ($\Omega_{III0} = 1$). Here in these regions we use homogeneous models locally because the ISW effect can be treated only in homogeneous models at present. We assume that these regions are connected by two infinitesimally thin walls at redshifts $z = 0.067$ and 0.45 corresponding to the boundary between I and II and the boundary between II and III, respectively. The latter redshift value 0.45 corresponds to a \sim Gpc radius of the spherical underdense region. The Hubble constants H_{I0} , H_{II0} and H_{III0} in these regions satisfy a relation $H_{I0} \geq H_{II0} \geq H_{III0}$. Here we consider the following two cases:

$$\begin{aligned} \text{case 1.} \quad & H_{I0} = 60, \quad H_{II0} = 50, \quad H_{III0} = 50 \text{ km/s/Mpc,} \\ \text{case 2.} \quad & H_{I0} = 70, \quad H_{II0} = 55, \quad H_{III0} = 50 \text{ km/s/Mpc,} \end{aligned} \quad (2.1)$$

where $H_{III0}(= 50)$ stands for the value necessary for the observed CMB anisotropies in the EdS model, $H_{I0}(= 70)$ in case 2 is the standard value in the local measurement, and the case 1 with smaller H_{I0} and H_{II0} is taken so as to consider a stringent observational condition which is given by the kinematic Sunyaev-Zeldovich effect[31].

If we regard the outer region as the background, the inner region can be interpreted as a local inhomogeneity and has an optical influence on the temperature of CMB radiation. If the observer is exactly at the center, the influence is isotropic, but if he is off-center, it brings dipole, quadrupole and the other multipole anisotropies. These anisotropies have already been analyzed and discussed in previous papers[41, 42, 43]. In what follows, we study the ISW effect due to small-scale density perturbations (of a simple spherical top-hat type) in the three regions in the inhomogeneous model.

In spherical coordinates (r, θ, ϕ) , the background metric of a constantly negatively curved spacetime in the inner regions I and II containing pressureless matter with a matter density ρ is given by

$$\begin{aligned} ds^2 &= a^2(\eta)(-d\eta^2 + dt^2), \\ dt^2 &\equiv \gamma_{ij}dx^i dx^j = dr^2 + \sinh^2(r)(d\theta^2 + \sin^2\theta d\phi^2), \end{aligned} \quad (2.2)$$

and

$$\begin{aligned} a(\eta) &= a_*(\cosh \eta - 1), \quad t = a_*(\sinh \eta - \eta), \\ \rho a^2 &= 3[(a'/a)^2 - 1] = 6/(\cosh \eta - 1), \end{aligned} \quad (2.3)$$

where t and η are the cosmic time and the conformal time. Prime ' represents $d/d\eta$ and a_* is a constant. The Hubble parameter, the density parameter and the redshift are

$$H_\alpha \equiv a'/a^2 = \frac{\sinh \eta_\alpha}{a_{\alpha*}(\cosh \eta_\alpha - 1)^2}, \quad \Omega_{\alpha m} = \frac{2}{\cosh \eta_\alpha + 1}, \quad z_\alpha + 1 = \frac{\cosh \eta_{\alpha 0} - 1}{\cosh \eta_\alpha - 1}, \quad (2.4)$$

where α is I or II, $\eta_{\alpha 0}$ is the present value of the conformal time η and for $a_{\alpha 0} \equiv a(\eta_{\alpha 0})$ we have $a_{\alpha 0}H_{\alpha 0} = \sinh \eta_{\alpha 0}/(\cosh \eta_{\alpha 0} - 1)$ and $\Omega_{\alpha m 0} = 2/(\cosh \eta_{\alpha 0} + 1)$. The constant a_* for region I or II is given by

$$a_{\alpha*} = \frac{\Omega_{\alpha m 0}}{2(1 - \Omega_{\alpha m 0})^{3/2}H_{\alpha 0}}, \quad (2.5)$$

where $H_{\alpha 0} = H_\alpha(\eta_{\alpha 0})$.

In the outer region III containing pressureless matter, the space-time metric is

$$ds^2 = a^2(\eta)[-d\eta^2 + \delta_{ij}dx^i dx^j], \quad (2.6)$$

where $a(\eta) \propto \eta^2$. The Hubble parameter, the density parameter and the redshift are $H_{III} \equiv a'/a^2 = 2/(\eta a)$, $\Omega_{III m} = 1$, and $z + 1 = (\eta_{III 0}/\eta)^2$. Here for $a_0 = a(\eta_{III 0})$ we have as $a_0 H_{III 0} = 2/\eta_{III 0}$.

For comparison, we consider a concordant flat FRW model with a cosmological constant Λ . The metric (2.2) is $dl^2 = \delta_{ij} dx^i dx^j$ and the scale factor satisfies $3(a'/a)^2 = (\rho_B + \rho_\Lambda)$, $6(a'/a)' = -(\rho_B - 2\rho_\Lambda)a^2$, where ρ_B and ρ_Λ are the energy density of matter and that of a cosmological constant Λ , respectively. As the model parameter of the concordant flat- Λ model, we adopt $\Omega_{m0} = 0.3$ and $H_0 = 70$ km/s/Mpc.

III. INTEGRATED SACHS-WOLFE EFFECT DUE TO DENSITY PERTURBATIONS

Now we consider growing mode of density perturbations and the integrated Sachs-Wolfe effect in the inner and outer regions, separately.

A. The inner regions I and II

The first-order gauge-invariant growing density perturbations ϵ_{mI} and the gauge-invariant potential perturbation (in the growing mode) $\Phi_A (= \Phi_H)$ [44] are expressed as

$$\begin{aligned}\epsilon_{Im} &= -G(\eta)\Delta F \\ \Phi_A &= -\frac{1}{2}\rho a^2 G(\eta)F\end{aligned}\quad (3.1)$$

with

$$\begin{aligned}G(\eta) &\equiv \frac{6}{\cosh \eta - 1} \left(1 - \frac{\eta(\cosh \eta + 1)}{2 \sinh \eta}\right) + 1, \\ &= \frac{1}{10}\eta^2 \left(1 - \frac{5}{84}\eta^2 + \dots\right) \quad \text{for } \eta \ll 1,\end{aligned}\quad (3.2)$$

where ϵ_{mI} corresponds to the density perturbations in the comoving synchronous gauge, Φ_A is equal to the potential perturbations $\phi^{(1)}$ in the longitudinal or Poisson gauge, and F is the potential function given as an arbitrary function of spatial coordinates. The expression of $G(\eta)$ was derived from the solution shown by Lifshits and Khalatinikov[45]. ΔF is the Laplacian of F in the space dl^2 , that is, $\Delta F = F|_i^i$, where $|i$ is covariant derivatives in the three dimensional space with γ_{ij} . So we obtain from Eqs.(2.3) and (3.1)

$$\phi^{(1)} = -\frac{3G(\eta)}{\cosh \eta - 1}F. \quad (3.3)$$

The first-order gauge-invariant temperature fluctuation due to the linear ISW effect is expressed as

$$\Delta T^{(1)}/T = -2 \int_{\lambda_o}^{\lambda_e} d\lambda \phi^{(1)} \quad (3.4)$$

in the Poisson gauge, where the prime is $\partial/\partial\eta$ and λ is the affine parameter along the light path. λ_e and λ_o are the emitter's and observer's values at the decoupling and present epochs, respectively.

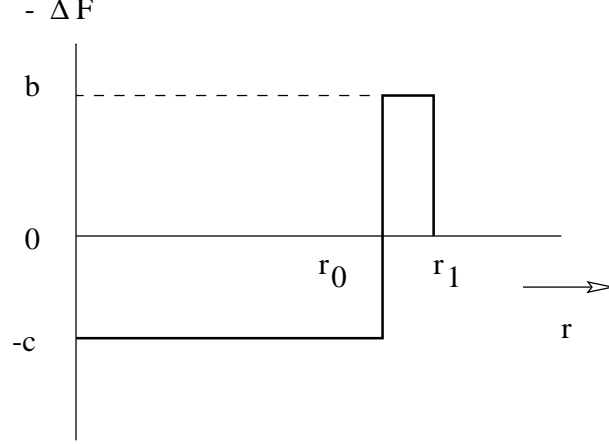
In this paper we consider a simple spherical top-hat type of compensated density perturbation following our previous paper[40], whose spatial size is much smaller than the horizon size. The spatial variation of the density perturbation is schematically shown in Fig.1. We consider the CMB photon paths passing through the center of the spherical perturbation. When the epoch in the center of the perturbation is η , the integral of $\phi^{(1)}$ along the light path reduces approximately to

$$(\Delta T/T)_\alpha = \Delta T^{(1)}/T = -\frac{6(\epsilon_{\alpha m 0})_c}{G(\eta_0)(\cosh \eta - 1)^3} [-(14 + \cosh \eta) \sinh \eta + 3\eta(2 \cosh \eta + 3)] \int_{\lambda_o}^{\lambda_e} d\lambda F/c, \quad (3.5)$$

where α is I or II, $(\epsilon_{\alpha m 0})_c$ and a constant c are the central values of $\epsilon_{\alpha m 0}$ and ΔF , respectively, and the subscript 0 denotes the present epoch. From integration of F for the above top-hat type perturbations derived in the previous paper[40], we obtain

$$(\Delta T/T)_\alpha = (\epsilon_{Im 0})_c \left(\frac{a_0 r_1}{(H_{I 0})^{-1}}\right)^3 \theta_\alpha,$$

FIG. 1: The matter density contrast for a top-hat type spherical void.



$$\theta_\alpha \equiv -\frac{4}{3} \frac{(1 - \Omega_{\alpha m 0})^{3/2}}{G(\eta_0)(\cosh \eta - 1)^3} [-(14 + \cosh \eta) \sinh \eta + 3\eta(2 \cosh \eta + 3)] w_1(y) \times \left(\epsilon_{\alpha m 0} / \epsilon_{I m 0} \right)_c \left(H_{\alpha 0} / H_{I 0} \right)^3, \quad (3.6)$$

where $w_1(y)$ is defined as $w_1(y) = -y \ln(1 + 1/y)$, $y = b/c$ and $r_1/r_0 = (1 + 1/y)^{1/3}$. For the value of y , we adopt $y = 0.5$ as an example.

B. The outer region III

The first-order ISW effect does not appear and the second-order ISW effect is the lowest one. The second-order temperature fluctuations were derived in our previous paper[40] and expressed as

$$\Delta T^{(2)}/T = \frac{4}{27} c^2 (r_1)^3 w_2(y) (\zeta_1 + 9 \zeta_2)', \quad (3.7)$$

where $w_2(y) \equiv y[1 - y \ln(1 + 1/y)]$, $(\zeta_1 + 9 \zeta_2)' = -(39/700)\eta$ for the EdS model, r_1 is the radius of inhomogeneities (cf. Fig. 1), and the central value of the density perturbation $(\epsilon_{III})_c$ is related to a constant c as

$$(\epsilon_{III})_c = -\frac{1}{20} \eta^2 c. \quad (3.8)$$

Using Eq.(3.8), the temperature fluctuations are expressed as

$$\begin{aligned} (\Delta T/T)_{III} &= \Delta T^{(2)}/T = -\frac{26}{63} \left(\frac{a_0 r_1}{(H_{III 0})^{-1}} \right)^3 \frac{(\epsilon_{III m 0})_c^2}{(1+z)^{1/2}} w_2(y), \\ &= (\epsilon_{I m 0})_c \left(\frac{a_0 r_1}{(H_{I 0})^{-1}} \right)^3 \theta_{III}, \\ \theta_{III} &\equiv -\frac{26}{63} \frac{(\epsilon_{III m 0})_c^2}{(\epsilon_{I m 0})_c (1+z)^{1/2}} \left(\frac{H_{III 0}}{H_{I 0}} \right)^3 w_2(y). \end{aligned} \quad (3.9)$$

The temperature fluctuations are negative definite. They are not exactly observed fluctuations, because their observed values should be the difference from the average value $\langle \Delta T^{(2)}/T \rangle$ of the sum of the second-order temperature fluctuations which is caused by all possible primordial density perturbations and renormalized into the background temperature. This average value is derived, taking account of power spectrum of density perturbations, in the procedure shown in a separate paper[46]. So the above $(\Delta T/T)_{III}$ should be here used to show the order of magnitude of second-order ISW effect, but for the perturbations with large amplitudes, the above second-order fluctuations are regarded approximately as observed values, as the mean value can be neglected.

C. The junction condition

The deformation of the walls brings the complicated perturbations inside the walls and their neighborhoods, as was studied by one of the present authors through the analysis of the junction condition[47]. They include not only density perturbations, but also gravitational-wave and rotational perturbations. Gravitational-wave perturbations propagate, but their amplitudes are very small and the contribution to density perturbations is negligible, because of the small coupling between them. Moreover the density and rotational perturbations caused by the perturbed walls do not propagate in the present dust matter models and are constrained in the just neighborhoods of the walls. In the most part of the I, II and III regions, therefore, we see density perturbations which are independent of the wall motions and were caused primordially due to the common origin.

Their amplitudes in the three regions were nearly equal at the early stages, but the present amplitudes became different, because they had different growth rates. Here we neglect the above complicated perturbations inside the walls and in their narrow neighborhoods. Then the three density perturbations $(\epsilon_{Im0})_c$, $(\epsilon_{IIIm0})_c$ and $(\epsilon_{IIIIm0})_c$ included in the two equations (3.6) and (3.9) are related as follows. First we assume that ϵ_{Im} , ϵ_{IIIm} and ϵ_{IIIIm} should be equal at early epochs of equal densities with the redshifts z_1, z_2 and $z_3 \gg 1$, i.e. $\epsilon_{Im}(z_1) = \epsilon_{IIIm}(z_2) = \epsilon_{IIIIm}(z_3)$, where $\rho_I(z_1) = \rho_{II}(z_2) = \rho_{III}(z_3)$. The present densities ρ_{I0}, ρ_{II0} and ρ_{III0} are related as $\rho_{I0}/\rho_{III0} = (\Omega_{I0}/\Omega_{III0})(H_{I0}/H_{III0})^2$ and $\rho_{II0}/\rho_{III0} = (\Omega_{II0}/\Omega_{III0})(H_{II0}/H_{III0})^2$. Then z_1, z_2 and z_3 are related as

$$\begin{aligned} (1+z_3)/(1+z_1) &= [\rho_{I0}/\rho_{III0}]^{1/3} = [(\Omega_{I0}/\Omega_{III0})(H_{I0}/H_{III0})^2]^{1/3}, \\ (1+z_3)/(1+z_2) &= [\rho_{II0}/\rho_{III0}]^{1/3} = [(\Omega_{II0}/\Omega_{III0})(H_{II0}/H_{III0})^2]^{1/3}. \end{aligned} \quad (3.10)$$

Taking account of the growth rates, we obtain $\epsilon_{Im0} = \epsilon_{Im}(z_1)G(\eta_{I0})/G(\eta_{I1})$, $\epsilon_{IIIm0} = \epsilon_{IIIm}(z_2)G(\eta_{II0})/G(\eta_{II2})$ and $\epsilon_{IIIIm0} = \epsilon_{IIIIm}(z_3)(1+z_3)$. Accordingly, we obtain

$$\begin{aligned} \epsilon_{IIIIm0} &= (1+z_3)\epsilon_{Im0}G(\eta_{I1})/G(\eta_{I0}), \\ \epsilon_{IIIIm0} &= (1+z_3)\epsilon_{IIIm0}G(\eta_{II2})/G(\eta_{II0}), \end{aligned} \quad (3.11)$$

where z and $G(\eta)$ are calculated using Eqs.(2.4) and (3.2). Here we set $z_1 = 1000$. Then we have $(\epsilon_{IIIIm0}/\epsilon_{Im0}, \epsilon_{IIIIm0}/\epsilon_{IIIm0})$ are (1.65, 1.15) and (1.83, 1.22) in cases 1 and 2, respectively.

D. Flat- Λ models

For comparison, we show the first-order and second-order temperature fluctuations in the flat- Λ models with $\Omega_m + \Omega_\Lambda = 1$, which were derived as $(\Delta T^{(1)}/T)_{loc}$ and $(\Delta T^{(2)}/T)_{loc}$ in our previous paper[40]. They are expressed as

$$\begin{aligned} (\Delta T^{(1)}/T)_{loc} &= (\epsilon_{Im0})_c \left(\frac{a_0 r_1}{(H_{I0})^{-1}} \right)^3 \theta_\Lambda^{(1)}, \\ \theta_\Lambda^{(1)} &\equiv \frac{4}{9} \left[\frac{2 \left(\frac{a'}{a} \right)^2 - \frac{a''}{a}}{\frac{a'}{a} P' - 1} \right]_0 \left(\frac{a'}{a} \right)_0^{-3} \left[\frac{a'}{a} + \left(\frac{a''}{a} - 3 \left(\frac{a'}{a} \right)^2 \right) P' \right] \left(\frac{\epsilon_{m0}}{\epsilon_{Im0}} \right)_c \left(\frac{H_0}{H_{I0}} \right)^3 w_1(y), \end{aligned} \quad (3.12)$$

and

$$\begin{aligned} (\Delta T^{(2)}/T)_{loc} &= (\epsilon_{Im0})_c \left(\frac{a_0 r_1}{(H_{I0})^{-1}} \right)^3 \theta_\Lambda^{(2)}, \\ \theta_\Lambda^{(2)} &\equiv \frac{16}{27} \left[\frac{2 \left(\frac{a'}{a} \right)^2 - \frac{a''}{a}}{\frac{a'}{a} P' - 1} \right]_0^2 \left(\frac{a'}{a} \right)_0^{-3} (\zeta_1 + 9\zeta_2)' \left(\frac{\epsilon_{m0}}{\epsilon_{m0I}} \right)_c \left(\frac{H_0}{H_{I0}} \right)^3 w_2(y), \end{aligned} \quad (3.13)$$

where ϵ_m and $(\epsilon_{m0})_c$ are first-order density perturbation and its central value at present epoch, and $P(\eta), Q(\eta), \zeta_1(\eta)$ and $\zeta_2(\eta)$ are auxiliary quantities used in the previous paper[40] and their definitions are shown in Appendix.

E. Analyses and results

In the following, we consider the behaviors of fluctuations due to the ISW effect in our inhomogeneous model in comparison with those in the concordant flat- Λ model.

To do so, we show the amplitudes of temperature anisotropy due to the ISW effect from a spherical compensating void/cluster with a given comoving radius and the density contrast, represented by the five quantities $\theta_I, \theta_{II}, \theta_{III}, \theta_\Lambda^{(1)}$ and $\theta_\Lambda^{(2)}$. Note that the first-order quantities θ_I, θ_{II} and $\theta_\Lambda^{(1)}$ do not depend on $(\epsilon_{Im0})_c$ and $(\epsilon_{m0})_c$, while the second-order ones θ_{III} and $\theta_\Lambda^{(2)}$ are proportional to $(\epsilon_{Im0})_c$ and $(\epsilon_{m0})_c$, respectively. Here c denotes the values at the centers of the voids/clusters. We assume that $(\epsilon_{m0})_c = (\epsilon_{Im0})_c$, so that the cosmological situation in the neighborhood of our observer in the flat- Λ model may be equal to that in the inner region I of the model.

In Fig. 2, we show the behaviors of θ_I, θ_{II} and $-\theta_{III}$ in the interval $0 < z < 1$, in cases 1 and 2, respectively. In Fig. 3, in a similar manner, we show the behaviors of θ_I, θ_{II} and $-\theta_{III}$ in the interval $0 < z < 10$, in cases 1 and 2, respectively. In these figures we adopted $(\epsilon_{m0})_c = (\epsilon_{Im0})_c = -0.37$, for which $-\theta_{III}$ is comparable with θ_I and θ_{II} , and $\theta_\Lambda^{(1)}$ is smaller than $-\theta_\Lambda^{(2)}$ for $z > 2.5$. For comparison, $\theta_\Lambda^{(1)}$ and $-\theta_\Lambda^{(2)}$ are also shown in them. Here the second-order quantities are multiplied by -1 , because they are negative definite and we use only positive quantities in the figures. From these figures, we can see that θ_I, θ_{II} and $\theta_\Lambda^{(1)}$ are comparable in the regions I and II, though their behaviors are different.

It is found that $|\theta_\Lambda^{(2)}|$ is smaller than $|\theta_{III}|$, though both quantities are of second-order. This reflects the strong dependence on the Hubble constants (cf. Eq.(3.9) and Eq.(3.13)) and the Λ -dependence of the second-order ISW effect which was studied in the previous paper[40].

As a result we find the following common features in cases 1 and 2 from these figures.

- (1) In the inner regions I and II, θ_I, θ_{II} and $\theta_\Lambda^{(1)}$ are comparable, irrespective of $r_1, (\epsilon_{Im0})_c$ and $(\epsilon_{m0})_c$, though θ_I and θ_{II} in case 1 seem to be larger by a factor ~ 1.5 than θ_I and θ_{II} .
- (2) In the outer region near the wall of $z = 0.45$, $|\theta_{III}|$ is roughly comparable with $\theta_\Lambda^{(1)}$ for $|(\epsilon_{Im0})_c| = 0.37$ and it is smaller or larger than $\theta_\Lambda^{(1)}$ for $|(\epsilon_{Im0})_c| <$ or > 0.37 , respectively. Far outside the wall, $|\theta_{III}|$ is larger than $\theta_\Lambda^{(1)}$.
- (3) Since $|\epsilon_{m0}|$ is ≈ 1 for perturbations with a size $L \approx 10h^{-1}\text{Mpc}$ ($H_0 = 100h \text{ km/s/Mpc}$), θ_{III} is extremely large or negligible compared with $\theta_\Lambda^{(1)}$ for perturbations with $L \ll 10h^{-1}$ or $\gg 10h^{-1}\text{Mpc}$, respectively.
- (4) First-order quantities θ_I, θ_{II} and $\theta_\Lambda^{(1)}$ are positive/negative for a cluster/void with $(\epsilon_{Im0})_c$ and $(\epsilon_{m0})_c$, respectively, while second-order quantities $|\theta_{III}|$ and $\theta_\Lambda^{(2)}$ are negative definite. Therefore, in the concordant model, the expected amplitude is larger for voids than clusters. Such an asymmetry is not expected in the outer region in our inhomogeneous model.
- (5) At epochs of $z < z_c (= 2.5 \text{ for } |(\epsilon_{m0})_c| \approx 0.37)$, $|\theta_\Lambda^{(2)}| < |\theta_\Lambda^{(1)}|$, so that the temperature fluctuations in the flat- Λ models have different signs for a cluster/void with a density contrast ϵ_{m0} . For $z > z_c$, however, the second-order ISW effect is dominant also in the flat- Λ model. Therefore, the temperature fluctuations in the flat- Λ models for $z > z_c$ is negative definite as in the outer region of our inhomogeneous models.

IV. CONCLUDING REMARKS

In this paper we studied the first-order and second-order ISW effect in our anti-Copernican inhomogeneous model with underdense regions in comparison with that in the concordant flat- Λ model. We found that a distinct feature appears at the outer region at moderate redshifts. In the concordant model, the expected amplitude of temperature anisotropy is larger for voids than clusters whereas such an asymmetry is not expected in the outer region in our inhomogeneous model. We showed, moreover, that the first-order ISW effect in the inner regions of our models is comparable with that in the flat- Λ model, and that the second-order ISW effect in the outer region depends on the amplitude ϵ_{m0} of density perturbations. The ISW effect due to perturbations on scales larger than $100h^{-1} \text{ Mpc}$ with a density contrast $|\epsilon_{m0}| < 0.37$ in the outer region is negligible. On the other hand, in the inner region, no ISW effect appears due to perturbations on scales larger than the radius of the inner region. In our inhomogeneous model with underdense regions, the ISW effect does not contribute to the low-multipole components of CMB anisotropies[7, 8] in accord with the assertion proposed by Hunt and Sarker[23], while in the flat- Λ model, the contribution from the ISW effect due to large-scale linear perturbations is significant.

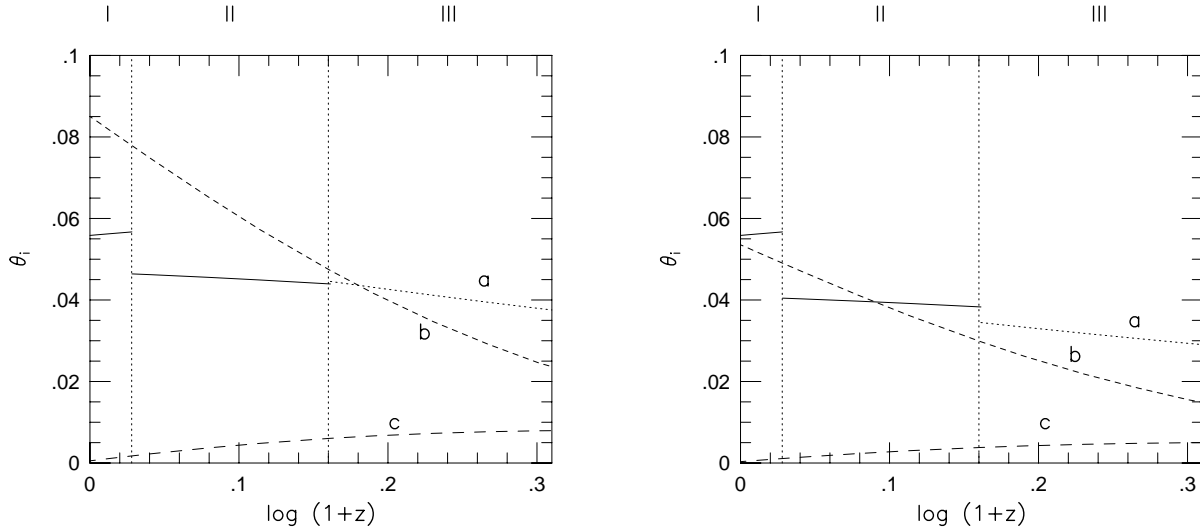


FIG. 2: The z -dependence of first and second order temperature fluctuations in case 1(left) and in case 2 (right) for photons passing through the center of a compensated spherical void at $z < 1$. Solid curves denote θ_I and θ_{II} and the curve a denotes θ_{III} . The curves b and c denote $\theta_{\Lambda}^{(1)}$ and $\theta_{\Lambda}^{(2)}$, respectively. The dotted vertical lines denote the boundaries at $z = 0.067$ and $z = 0.45$. We adopted $(\epsilon_{m0})_c = (\epsilon_{Im0})_c = -0.37$, for which $-\theta_{III}$ is comparable with θ_I and θ_{II} .

The observed correlation between the CMB sky with the large-scale structure is usually interpreted as the evidence of the cosmological constant Λ , which causes the first-order ISW effect[9, 10]. Recently, moreover, hot and cold spots on the CMB sky associated with super-structures (with $z \sim 0.5$) in SDSS Luminous Red Galaxy catalog were measured by Granett et al.[11] and the consistency with the ISW effect in the flat- Λ models was shown. It should be noted, however, that they may be brought in principle by the first and second-order ISW effect also in our models with underdense regions, as we showed in the present paper. Therefore, the observational evidence for the existence of small-scale ISW effect for light paths through clusters of galaxies, superclusters and supervoids may support not only the flat- Λ model, but also our models with underdense regions.

In order to make a clear distinction between the two models, it is better to compare the overall amplitudes of temperature fluctuations associated with a void(negative density) with those associated with a cluster(positive density). As we have seen, for $0.45 < z < z_c$ (which depends on ϵ_{m0}), the amplitudes for quasi-linear voids are larger than those for quasi-linear clusters in the concordant model due to the second-order effect, while such an asymmetry cannot be expected in our inhomogeneous model since there is no first-order effect in the outer region[40, 48].

APPENDIX A: DEFINITIONS OF $p(\eta)$, $q(\eta)$, $\zeta_1(\eta)$ AND $\zeta_2(\eta)$

$P(\eta)$ satisfies

$$P'' + \frac{2a'}{a}P' - 1 = 0 \quad (\text{A1})$$

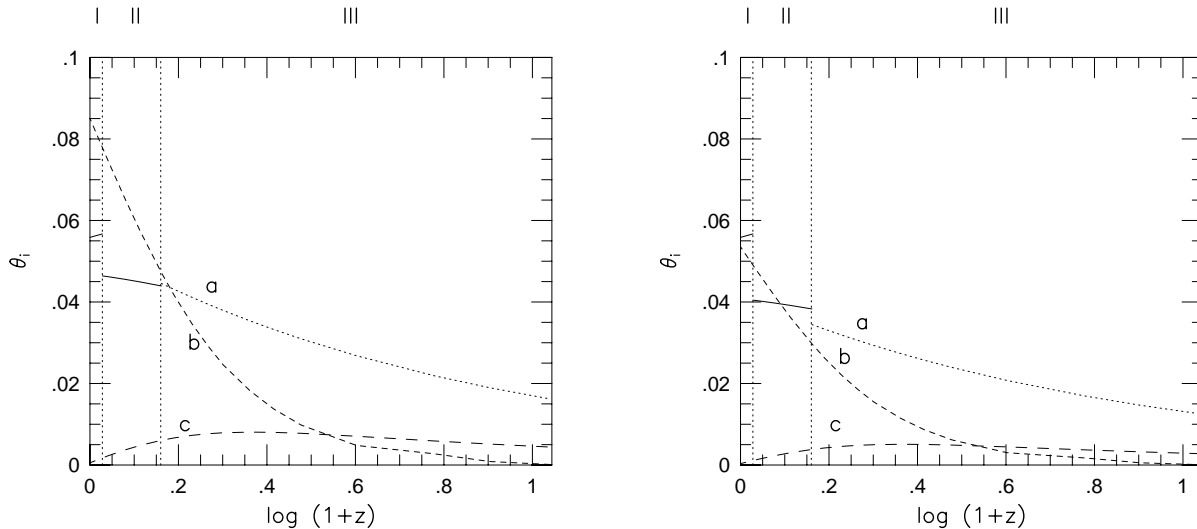


FIG. 3: The z -dependence of first and second order temperature fluctuations in case 1(left) and in case 2 (right) for photons passing through the center of a compensated spherical void at $z < 10$. Solid curves denote θ_I and θ_{II} and the curve a denotes θ_{III} . The curves b and c denote $\theta_{\Lambda}^{(1)}$ and $\theta_{\Lambda}^{(2)}$, respectively. The dotted vertical lines denote the boundaries at $z = 0.067$ and $z = 0.45$. We adopted $(\epsilon_{m0})_c = (\epsilon_{Im0})_c = -0.37$, for which $-\theta_{III}$ is comparable with θ_I and θ_{II} .

and its solution is expressed as

$$\begin{aligned}
 P(\eta) &= -\frac{2}{3\Omega_{m0}} a^{-3/2} [\Omega_{m0} + \Omega_{\Lambda 0} a^3]^{1/2} \int_0^a d\tilde{a} \tilde{a}^{3/2} [\Omega_{m0} + \Omega_{\Lambda 0} \tilde{a}^3]^{-1/2} + \frac{2}{3\Omega_{m0}} a, \\
 \eta &= \int_0^a d\tilde{a} \tilde{a}^{-1/2} [\Omega_{m0} + \Omega_{\Lambda 0} \tilde{a}^3]^{-1/2}.
 \end{aligned} \tag{A2}$$

The functions ζ_1 and ζ_2 are defined as

$$\begin{aligned}
 \zeta_1 &= \frac{1}{4} P \left(1 - \frac{a'}{a} P' \right), \\
 \zeta_2 &= \left\{ \frac{1}{21} \frac{a'}{a} \left(P P' - \frac{1}{6} Q' \right) - \frac{1}{18} \left[P + \frac{1}{2} (P')^2 \right] \right\},
 \end{aligned} \tag{A3}$$

where $Q(\eta)$ is satisfies

$$Q'' + \frac{2a'}{a} Q' = - \left[P - \frac{5}{2} (P')^2 \right]. \tag{A4}$$

-
- [1] B.P. Schmidt et al., *Astrophys. J.* **507**,46 (1998).
 - [2] A.G. Riess et al., *Astron. J.* **116**,1009 (1998).
 - [3] A.G. Riess et al. *Astron. J.* **118**,2668 (2000).
 - [4] S. Perlmutter et al., *Astrophys. J.* **517**,565 (1999).
 - [5] C.L. Bennet et al., *Astrophys. J. Suppl.* **148**, 1 (2003).

- [6] D.N. Spergel et al., *Astrophys. J. Suppl.* **148**, 175 (2003).
- [7] A. de Oliveira-Costa et al., *Phys. Rev.* **D69**, 063516 (2004).
- [8] C.R. Contaldi et al., *J. Cosmol. Astropart. Phys.* **7**, 2 (2003).
- [9] S. Boughn and R. Crittenden, *Nature* **427**,45 (2004)
- [10] R.G. Crittenden and N. Turok, *Phys. Rev. Lett.* **76**, 575 (1966).
- [11] B.R. Granett, M.C. Neyrinck and I. Szapudi, arXiv:0805.3695.
- [12] M.N. C el erier, *Astron. Astrophys.* **353**,63 (2000); astro-ph/9907206; M.N. C el erier, *New Adv. Phys.* **1**,29 (2007).
- [13] S.P. Goodwin, A.J. Barber, J. Griffin and L.I. Onuora, astro-ph/9906187.
- [14] K. Tomita, *Astrophys. J.* **529**, 26 (2000); astro-ph/9905287.
- [15] K. Tomita, *Astrophys. J.* **529**, 38 (2000); astro-ph/9906027.
- [16] K. Tomita, *MNRAS* **326**, 287 (2001)
- [17] K. Tomita, *Prog. Theor. Phys.* **106**, 929 (2001).
- [18] H. Alnes, M. Amarzguioui and O. Gron, *Phys. Rev.***D73**, 083519 (2006); H. Alnes and M. Amarzguioui, *Phys. Rev.***D75**, 023506 (2007).
- [19] T. Biswas, R. Mansouri and A. Notari, *J. Cosmol. Astropart. Phys.* **12**, 017 (2007).
- [20] S. Alexander, T. Biswas, A. Notari and D. Vaid, arXiv:0712.0370.
- [21] H. Iguchi, T. Nakamura and K. Nakao, *Prog. Theor. Phys.* **108**, 809 (2002).
- [22] A. Blanchard et al., *Astron. Astrophys.* **412**, 35 (2003).
- [23] P. Hunt and S. Sarkar, *Phys. Rev.* **D76**, 123504 (2007); arXiv:0706.2443.
- [24] D.J. Eisenstein et al., *Astrophys. J.* **633**,560 (2005).
- [25] H.-J. Seo and D.J. Eisenstein, *Astrophys. J.* **598**,720 (2003).
- [26] W.J. Percival et al., *MNRAS* **381**,1053 (2007).
- [27] W.J. Percival et al., *Astrophys. J.* **657**,51 (2007).
- [28] W.J. Percival et al., *Astrophys. J.* **657**,645 (2007).
- [29] E. Gazta naga, R. Miquel and E. S anchez, arXiv:0808.1921.
- [30] J.P. Zibin, A. Moss and D. Scott, arXiv:0809.3761.
- [31] J. Garc a-Bellido and T. Haugb olle, arXiv:0807.1326.
- [32] R.R. Caldwell and A. Stebbins, arXiv:0711.3459.
- [33] T. Clifton, P.G. Ferreira and K. Land, arXiv:0807.0443.
- [34] J. Garc a-Bellido and T. Haugb olle, *J. Cosmol. Astropart. Phys.* **4**, 3 (2008).
- [35] K. Tomita, *Phys. Rev.* **D71**, 083504 (2005).
- [36] K. Tomita, *Phys. Rev.* **D72**, 043526 (2005).
- [37] K. Tomita, *Phys. Rev.* **D72**, 103506 (2005).
- [38] K.T. Inoue and J. Silk, *Astrophys. J.* **648**, 23 (2006).
- [39] K.T. Inoue and J. Silk, *Astrophys. J.* **664**, 650 (2007).
- [40] K. Tomita and K.T. Inoue, *Phys. Rev.***D77**, 103522 (2008).
- [41] K. Tomita, *Astrophys. J.* **584**, 580 (2003).
- [42] J.W. Moffat, *J. Cosmol. Astropart. Phys.* **10**, 12 (2005).
- [43] H. Alnes and M. Amarzguioui, *Phys. Rev.***D74**, 103520 (2006).
- [44] J.M. Bardeen, *Phys. Rev.***D22**, 1882 (1980).
- [45] E.M. Lifshitz and I.M. Khalatnikov, *Adv. Phys.* **12**, 185 (1963).
- [46] K. Tomita, *Phys. Rev.***D77**, 103521 (2008).
- [47] K. Tomita, *Phys. Rev.***D70**, 123502 (2004).
- [48] N. Sakai, K.T. Inoue, *Phys. Rev.* **D78**, 063510 (2008).